

Dynamic Control of Laser Produced Proton Beams

**S. Kar[‡], K. Markey, P.T. Simpson, B. Dromey, M. Borghesi,
M. Zepf**

The Queen's University of Belfast, Belfast BT7 1NN, UK

**C. Bellei, S.R. Nagel, S. Kneip, L. Willingale, Z. Najmudin, K.
Krushelnick[§]**

Blackett Laboratory, Imperial College, London, SW7 2BW, U.K.

J.S. Green, P. Norreys, R.J. Clarke, D. Neely

Central Laser Facility, Rutherford Appleton Laboratory, Chilton, OX11 0QX, U.K.

D.C. Carroll, P. McKenna

SUPA, Department of Physics, University of Strathclyde, Glasgow, G4 0NG, U.K.

E.L. Clark

Department of Electronics, Technological Educational Institute of Crete, Chania,
Crete, Greece

Abstract.

The emission characteristics of intense laser driven protons are controlled using ultra-strong (of the order of 10^9 V/m) electrostatic fields varying on a few ps timescale. The field structures are achieved by exploiting the high potential of the target (reaching multi-MV during the laser interaction). Suitably shaped targets result in a reduction in the proton beam divergence, and hence an increase in proton flux while preserving the high beam quality. The peak focusing power and its temporal variation are shown to depend on the target characteristics, allowing for the collimation of the inherently highly divergent beam and the design of achromatic electrostatic lenses.

PACS numbers: 52.38.Ph, 41.75.Jv, 41.85.Ne, 52.59.-f

[‡] Electronic address: s.kar@qub.ac.uk

[§] Currently at CUOS, University of Michigan, Ann Arbor 48109, USA

1. Introduction

One of the most dynamic fields in arena of particle acceleration has been the area of laser-plasma based accelerators [1, 2, 3, 4, 5, 6]. This rapid development and world-wide interest is driven by the fact that far larger accelerating gradients can be exploited than in conventional accelerators (in excess of 10^{12} V/m [6] compared to 10's of MeV/m in conventional designs). Consequently, laser driven accelerators hold the promise of compact accelerating structures, which may be advantageous for a number of applications [7]. After only a very short period of development laser-accelerated proton beams [4, 5] have been shown to have very small longitudinal and transverse emittance [8, 9]. However, the excellent emittance is the result of a very short initial burst duration and a very small virtual source size. By extension the proton beam emerging from the target has a broad energy spectrum (100% up to E_{max}) and large, energy dependent, divergence angle (typically 40 - 60 deg depending on laser and target parameters). The manipulation of laser generated proton beams gives new challenges due to the high bunch charge and short pulse nature of the beams, requiring innovative approaches to enable beam control - recently a technique employing electric fields triggered by a second laser pulse on a separate target, has been used for focusing selectively a portion of the beam spectrum [10]. However, the inherent large divergence and energy spread can make it hard to utilise the full flux of the proton beam for applications and indeed for further transport and beam manipulation. Here we demonstrate a novel target configuration which, without the need for an auxiliary laser pulse, exploits the self-charging of the target to improve the collimation of the entire proton beam, while conserving the characteristic high laminarity required for radiography applications [11]. This approach also allows the control of chromatic properties of the beam and creation of achromatic electrostatic lenses, by exploiting the strong temporal variation of the target potential. Hence this technique allows the full flux of the proton beam to be used in many demanding applications in science, medicine and industry [7].

In high power laser interactions with solid targets, a significant fraction of the laser energy gets transferred to the hot electron population. Above a peak laser intensity 10^{19} W cm⁻², experiments [12] and particle-in-cell simulations [13] have reported laser-to-electron conversion efficiencies up to 50%. Most of the absorbed energy is carried by the forward moving hot electron population with an electron spectrum that can be approximated as an exponential $dN/dE = (N_0/U_p) \times e^{-E/U_p}$, with a temperature of the order of the ponderomotive potential of the incident laser [$U_p = 0.511 \times (\sqrt{1 + (a_0^2/2)} - 1)$ MeV, where a_0 is the normalized laser vector potential]. A small fraction of the hot electron population escapes and rapidly charges the target to a potential of the order of U_p preventing the bulk of the hot electrons from escaping. The time dependence of the target potential is governed by the self-capacitance of the target (C_T). At a given time t , the number of electrons that have escaped from the target is given by $N_{es}(t) = N_0 \times e^{-E_{cutoff}(t)/U_p}$ which satisfies the equation, $eN_{es}(t)/C_T(t) = 10^{-6} \times E_{cutoff}(t)$. Here

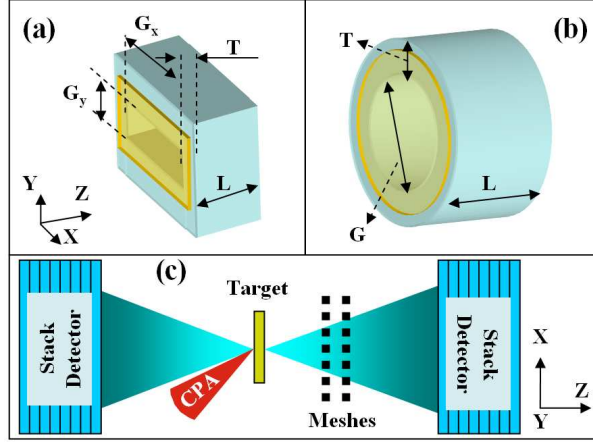


Figure 1. Schematic of (a) rectangular and (b) cylindrical lens-targets fielded in the experiment. (c) Schematic of the experimental setup (top view).

e is electron charge and E_{cutoff} is the cut-off energy (in MeV) of the confined electron spectrum. Assuming the lateral velocity of the charge wave equals to $0.75c$ [14], the time dependent target self-capacitance can be estimated as that of a disk of increasing radius $C_T(t) \sim 8\epsilon_0(r_0 + 0.75ct)$, where ϵ_0 is permittivity of vacuum and r_0 the laser spot size on the target. From these considerations it follows that the target potential remains above several MV for all relevant time scales considered here. Targets charged to similar potentials have been shown to produce substantial transverse deflections of multi-MeV proton beams [15]. Suitable design of the target geometry (as shown later) therefore enables a strong electrostatic lens to be created.

2. Experimental Setup

The experiment was performed at Rutherford Appleton Laboratory employing VULCAN Petawatt laser system. The laser pulse delivered $\sim 300\text{J}$ of energy on target in 500-600 fs FWHM duration. Using an $f/3$ off-axis parabola, the laser was focussed to $8\text{ }\mu\text{m}$ FWHM spot with a peak intensity $\sim 10^{21}\text{ W cm}^{-2}$. Two basic shapes of electrostatic lens geometries, rectangular and cylindrical (Fig. 1(a-b)) were investigated and compared to the performance of flat Au foil targets. For all shots the laser interacted with a $15\text{ }\mu\text{m}$ thick Au foil at its centre, at an angle of incidence of 40 degrees from target normal. All targets were mounted on ~ 3 millimeter thick and ~ 2 centimeters long plastic stalks in order to provide a highly resistive path to the current flowing from target to ground. Spatial and spectral profiles of the multi-MeV proton beam emitted normally from either side of the target were measured by employing stacks of radiochromic films (a dosimetry detector [16]) as shown in Fig. 1(c). The dose response of the RCF detectors were calibrated by exposing them to various known doses of protons from a linear accelerator [17]. In some shots, Cu sheets of suitable thickness were inserted in the stacks in order to obtain proton spectrum via activation

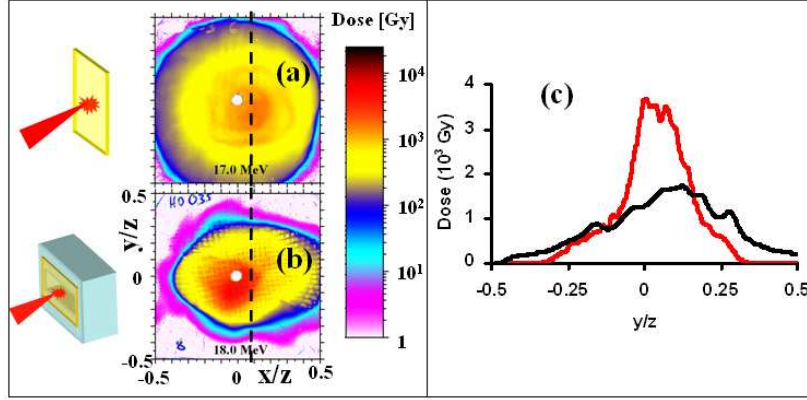


Figure 2. Experimentally obtained proton beam (of energies 17.5 MeV) spatial dose profiles for (a) plain foil target and (b) a Al rectangular lens-target of $G_x=5$ mm, $G_y=1$ mm, $L=2$ mm and $T=0.5$ mm. Spatial scales of the images are normalized to their distances from the proton generating foil. (c) Lineouts along the dotted line in (a) (black) and (b) (red) are shown.

measurements [18], complementary to those obtained from RCF dose measurements. Multiple periodic meshes were introduced at the rear side of the proton generating target, at various distances from it. Multiple mesh radiographs enable virtual proton source measurement [8], as well as to map the proton trajectories.

3. Experimental results and analysis

Significant (up to a factor of two) reductions in the proton beam divergence angle were observed in case of the lens-targets when compared to free-standing flat foils. The angular divergence of the low energy part (up to 25 MeV) of the spectrum was observed to be highly reproducible ($\sim 56^\circ$) for the flat foil targets (typical proton beam profile is shown in Fig. 2(a)). In order to ensure that the observed effect was unambiguously due to the target geometry, rectangular lens-targets (see Fig. 1(b)) were employed. Fig. 2(b) shows a 2D flux profile of the proton beam obtained from a rectangular lens-target. Instead of the typical near-circular beam profile, an elliptical profile (with a major to minor axes ratio of up to 2:1 as shown in Fig. 2(b)) is observed. Only the divergence of protons that have propagated through the lens is affected (i.e. the protons propagating towards the laser are not affected by the modified target geometry). Mounting the rectangular lens on the front surface of the proton generating foil, resulted in an elliptical spatial profile of the proton beam propagating towards the laser. As expected in this case, the proton beam from the rear side of the target retains a spatial dose profile similar to that from flat foil target. Employing lens-targets with cylindrical symmetry (Fig. 1(b)), resulted in a near-circular profile of rear side protons (Fig. 3) with significant reduction in beam divergence as compared to the flat foil case.

The spectral shape and overall dose is not affected by the addition of a lens element

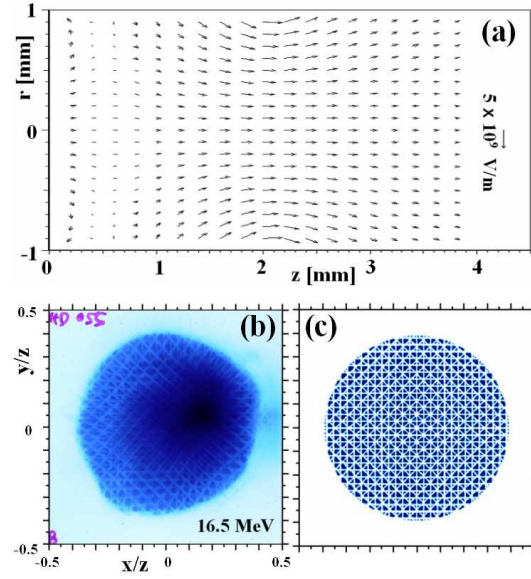


Figure 3. (a) Longitudinal (across XZ plane) electric field profile across a cylindrical Al lens-target of $G=2$ mm, $L=2$ mm and $T=0.5$ mm. Experimental (b) and simulated (c) proton spatial dose profiles (mainly due to 16.5 MeV protons) obtained from the cylindrical lens-target. Spatial scales of the images are normalized to their distances from the proton generating foil.

to the target geometry. Spatially integrated proton beam spectra from both plain foil and lens-targets agree to within the typical shot to shot variations. Consequently an increase in the proton flux commensurate with the reduction in beam size is seen in the case of lens-targets with respect to the plain foil case (for example, see Fig. 2(c)). Moreover, no significant change in the proton beam cut-off energy was found in case of the lens-targets in comparison to the plain foil targets. This suggests that the accelerating fields are not affected by the addition of a lens structure. This is in good agreement with expectations since the time it takes for the charge wave to spread to the lens far exceeds the proton acceleration time [14].

3D particle tracing simulations, employing PTrace [19], were carried out in order to study the focussing due to the electrostatic lens formed by the self-charging of the target. The temporal evolution of the target potential is calculated by considering the self-capacitance of a charged disk of radius $r_0 + 0.75ct$ and an exponential electron distribution with a temperature of U_P as described above. The potential of the target is assumed constant after the charge wave reaches the end of the lens at a time t_{ss} , such that $r_0 + 0.75ct_{ss} = G/2 + L$ (G and L are the inner diameter and length of the cylindrical lens as shown in Fig. 1(b)). The electric field at a given point and at a given time is obtained by superimposing the contributions from every part of the charged target. Test particles (protons) are launched from a point source with a divergence and initial position taken from experimental observations on shots with a flat foil. As shown in the Fig. 3(a), the steady state electric field profile due to a circular lens-target

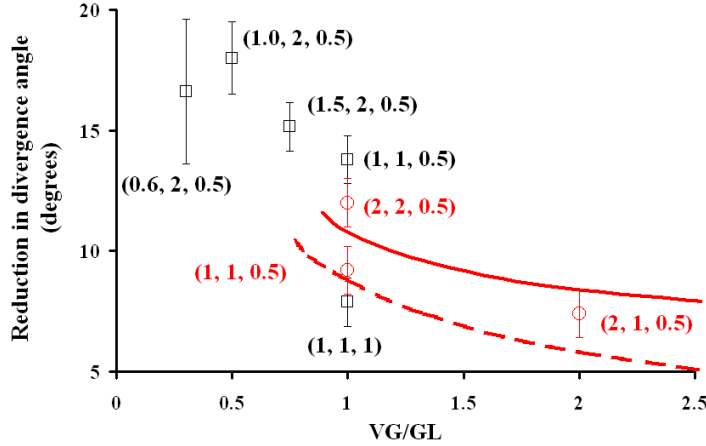


Figure 4. Experimentally obtained data points showing reduction in proton beam (of 17.5 MeV) divergence (along Y axis) due to rectangular (square) and cylindrical (circle) aluminum lens-targets of different dimensions. Dimensions (in mm) of the rectangular(cylindrical) targets are mentioned as $[G_y(D), L, T]$, next to the respective data points. All rectangular lens-targets had $G_x=5$ mm. Solid(dotted) lines are simulated values for 0.5 micron thick cylindrical lens-targets of G_y equals to 2 mm(1 mm).

fielded in the experiment resembles that of a conventional electrostatic *Einzell* lens and therefore acts to reduce the proton beam divergence by the strong transverse field near the edge of the charged lens-target. Since the proton beam is strongly divergent inside the lens the longitudinal field also contributes to the collimation of the beam.

As shown in Fig. 3(b) and (c), the simulated proton beam parameters at the detector plane closely match the experimentally observed beam in both the overall dimension (divergence) as well as the mesh magnification. Good agreement between model and observation was obtained across different energies and for all circular lens-targets as shown in Fig 4.

Both the simulations and the experimental data show no significant loss of intrinsic proton beam emittance. This is demonstrated by the clearly visible radiographs of the mesh (both experimentally as well as in the simulations). Radiographs taken with two meshes confirm that the that the protons follow straight line trajectories outside the focussing field region.

From the comparison of simple Einzel-lens type configuration it is clear that the properties of the proton beam can be manipulated effectively. From the presented data it is clear that compensating for the residual divergence (around 20 degrees) could be achieved with a secondary lens target [10] and result in a beam collimated to a diameter of a few mm size. The strong role that the detailed geometry plays can be seen in Fig. 4, where the reduction in the proton beam divergence for a number of lens-targets of different geometries is shown. Collimation increases with decreasing aspect ratio G_y/L for the rectangular lens (or G/L for the cylindrical case) and decreases with increasing

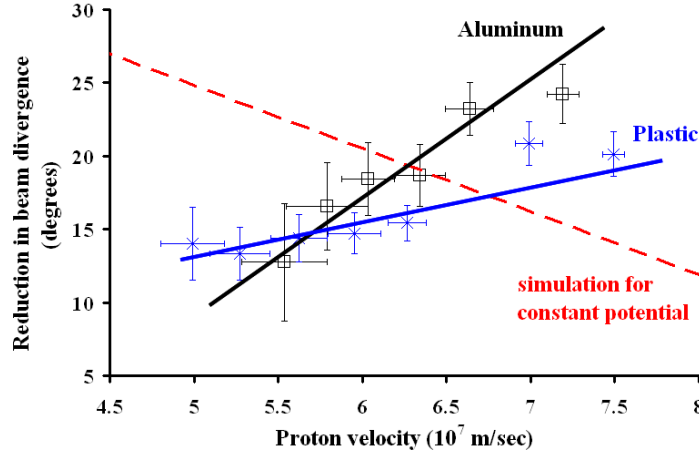


Figure 5. Trend (solid line) of reduction in divergence over different proton beam energy for two rectangular ($G_x=5$ mm, $G_y=0.6$ mm, $L=2$ mm and $T=0.5$ mm) lens targets of different materials, mentioned next to the respective trend lines. Red dashed line illustrates chromatic behaviour of a simulated static electrostatic lens.

wall thickness T . These effects are consistent with the higher fields obtained for a given potential for smaller structures, changes in the interaction length and variations in target capacitance respectively. Clearly, modifying the geometry towards more complex shapes may also yield improved collimation/focusing performance.

So far we have only discussed the behaviour of the proton beam at a given proton energy. However, the focusing strength of an electrostatic lens varies strongly with beam energy - i.e. it is chromatic. Harnessing the full potential of these beams (e.g. by focusing them to one spot or coupling the whole bunch into a post-accelerator or phase-rotator) requires that the chromatic behaviour be addressed. The dynamic charging and discharging of the investigated structures allow a significant control of the chromatic behaviour of the electrostatic lens. As the charge wave spreads at much higher speed than the protons, complete charging up of the target is attained much earlier than the protons leave the active focussing field region. The protons are therefore still in the field of the lens during the discharging period. The target discharges primarily due to the current flowing through the stalk holding the target. In our case, abrupt discharging of the lens target was avoided by employing insulating stalks. Clearly the discharge time scale will also be a function of the lens material. As shown in Fig. 5 the Aluminium targets discharge (and hence lose their focusing field) much more rapidly than the plastic targets. For our geometry the discharge time constant for the Aluminium lens was roughly 7.5 ps, resulting in substantial drop of the lens potential during the particle transit. Consequently, the slower particles see a reduced collimating field and experience a smaller reduction in beam divergence. Note that for a constant potential the slower protons would experience a larger drop in beam divergence inversely proportional to the proton velocity (see Fig. 5). In the case of the plastic lens the discharge time is clearly much longer (~ 15 ps). In this case the slower reduction in lens potential almost

perfectly compensates the enhanced collimation expected at lower energies for constant lens potential, resulting in an achromatic collimating system. Clearly, similar approaches can be taken to achieve achromatic focusing or a compensation of the initial chromatic dependency of the proton beam divergence. For example mounting the target with much thinner (few microns) insulating wires is expected to result in negligible discharging of the target during the relevant time scale [20], resulting in significant improvement in lower energy proton beam collimation.

4. Possible Advancements

Indeed, further improvement in the beam collimation can be achieved by suitably modified lens-target designs. For instance, reducing the wall thickness (T) from 0.5 mm to $50\mu\text{m}$ will substantially increase the surface charge density. Similarly, the observed increase in beam collimation with longer L and shorter G suggests, a conical (instead of cylindrical) lens geometry will produce stronger focussing by guiding the beam optimally from its source. For example, in case of a 30 degree conical lens-target with initial diameter of 0.4 mm, $L=2$ mm and $T=50\mu\text{m}$, simulations predict in excess of factor of three reduction of few MeV proton beam divergence for the discussed experimental conditions. This implies an order of magnitude increase in the proton flux which would be promising for high energy density physics and fusion research.

5. Conclusions

In conclusion, we have shown that by careful choice of target geometry an electrostatic lens can be formed which improves the collimation of the protons emitted from a laser irradiated foil target. Significant reductions in the beam divergence and commensurate increase in flux have been observed without sacrificing the high beam quality in excellent agreement with 3D particle tracing simulations. In addition, it is possible to offset the chromatic nature of an electrostatic lens with the discharging of the lens structure allowing for near-achromatic lens performance and a route for correcting chromatic aberrations inherent in the proton beam production process.

6. Acknowledgements

This work is funded by EPSRC. M.Zepf is the holder of a Royal Society Wolfson Merit Award. Authors acknowledge supports from the target fabrication group of RAL. SK would like to thank Dr. A. Schiavi for the code PTRACE.

7. References

- [1] S.P.D. Mangles *et al.*, Nature, **431**, 535 (2004).
- [2] C.G.R. Geddes *et al.*, Nature, **431**, 538 (2004).
- [3] J. Faure *et al.*, Nature, **431**, 541 (2004).

- [4] E. Clark *et al.*, Phys. Rev. Lett., **84**, 670 (2000).
- [5] R. Snavely *et al.*, Phys. Rev. Lett., **85**, 2945 (2000).
- [6] B.M. Hegelich *et al.*, Nature, **439**, 441 (2006)
- [7] M. Borghesi *et al.*, Fusion Sci. Tech., **49**, 412 (2006).
- [8] M. Borghesi *et al.*, Phys. Rev. Lett., **92**, 55003 (2004).
- [9] T.E. Cowan *et al.*, Phys. Rev. Lett., **92**, 204801 (2004).
- [10] T. Toncian *et al.*, Science, **312**, 410 (2006).
- [11] A. Mackinnon *et al.*, Phys. Rev. Lett., **97**, 045001 (2006).
- [12] K.B. Wharton *et al.*, Phys. Rev. Lett., **81**, 822 (1998).
- [13] S.C. Wilks *et al.*, IEEE J. Quant. Electron., **33**, 1954 (1997).
- [14] P. McKenna *et al.*, Phys. Rev. Lett., **98**, 145001 (2007).
- [15] M. Borghesi *et al.*, Appl. Phys. Lett., **82**, 1529 (2003).
- [16] M. Borghesi *et al.*, Phys. Plasmas, **9**, 2214 (2002).
- [17] T. Toncian, Private communication.
- [18] P. McKenna *et al.*, Phys. Rev. E, **70**, 036405 (2004).
- [19] A. Schiavi, Ph.D. Thesis, Imperial College, London, U.K. (2003).
- [20] S.D. Baton *et al.*, High Energy Density Phys.(2007), doi:10.1016/j.hedp.2007.05.002.
- [21] P. Patel *et al.*, Phys. Rev. Lett., **91**, 125004 (2003).